ARTICLE

Tunability of Mobility and Conductivity over Large Ranges in Poly(3,3‴-didodecylquaterthiophene)/ Insulating Polymer Composites

J. Sun, B.-J. Jung, T. Lee, L. Berger, J. Huang, Y. Liu, D. H. Reich, and H. E. Katz*

Department of Materials Science and Engineering, Johns Hopkins University, 103 Maryland Hall, 3400 North Charles Street, Baltimore, Maryland 21218

ABSTRACT Semiconducting polymers are currently being considered as active layers in field-effect transistors, in which high charge carrier mobility and low off conductivity are important. For other applications, such as certain spintronic mechanisms, the opposite characteristics are desirable. Blending such polymers with insulating polymers would be expected to lower the mobility. In this paper, we report that the use of hydrocarbon polymers such as polystyrene as insulators generally raises the mobility when the semiconducting polymer is poly(bisdodecylquaterthiophene). A high mobility value of nearly 0.1 $cm^2/V \cdot s$ was obtained for an optimal blend. While this is counterintuitive, it is consistent with a few other recent reports. In order to lower the mobility significantly, a much more polar and irregular blending agent is needed. The further addition of tetrafluorotetracyanoquinodimethane as a dopant gave a rare low mobility/high conductivity combination of properties, with a charge carrier density on the order of 10^{19} cm^{-3}. Thus, mobility and conductivity were tuned somewhat independently over 3 and 4 orders of magnitude, respectively.

KEYWORDS: PQT-12 • polymer blend • transistor • conductivity • mobility

INTRODUCTION

Solution-processable conjugated polymers enable low-cost liquid-phase deposition techniques (spin coating, inkjet printing, and screen printing) for conductors and semiconductors, and are being considered for many applications, including fabrication of large area (active matrix displays), light-emitting diodes, polymer solar cells, and compact, lightweight, flexible active circuits (1−7). Regioregular polythiopenes constitute an interesting class of model conjugated polymers for the study of oxidative stability, self-assembly capability, and performance in field-effect transistors (FETs) (8−11). Recently, a series of studies has focused on solution blending of polythiophenes and insulating polymers in order to reduce cost, improve stability via self-encapsulation (12), and enhance mechanical properties. These blends in FETs would be expected to show diminished electronic performance relative to pure polymers. However, a few recent results demonstrate the opposite: that blending of polythiophenes with an insulating polymer can improve the device performance. For example, Lu et al. reported that the conductivity of the composite can be enhanced upon mixing of highly crystallized poly(3-butylthiophene) with insulating polymers such as amorphous polystyrene (a-PS) or poly(methyl methacrylate) (PMMA) (13); Goffri et al. reported that the mobility remains almost the same in composites of the conjugated polymer poly(3-hexylthiophene) (P3HT) and the insulating polymer (isotactic semicrystalline i-PS) over a rather wide ratio compared to pure conjugated polymer (14). Mobilities are kept within the range of 0.02−0.09 $cm^2/V \cdot s$ in a series of P3HT/PMMA diblock copolymers with various block length ratios (15). The advantage of such an approach is seen as improved formulation of the latitude of printing, improved cost effectiveness, and greater control over the morphology of the organic semiconductor active layer (16).

Besides mobility, polythiophene polymers, which generally have donor character, can blend with the very strong molecular electron-acceptor tetrafluorotetracyanoquinodimethane (F4TCNQ) to increase the conductivity. An especially high conductivity (1 S/cm) has been reported (17, 18). However, it is not known how much of the conductivity increase can be attributed to the charge density created by doping and how much to higher hole mobility. In fact, a low mobility with high conductivity in a thiophene polymer blend has never been rigorously shown, although in one particular application of interest to us this combination may be advantageous.

In spin-precession magnetic sensor devices, polymers with decidedly low mobility ($\sim 10^{-6}$−10^{-5} $cm^2/V \cdot s$) and very high carrier concentration (10^{17}−10^{19} cm^{-3}) are required to enhance the detectivity to nearly that of the SQUID but at room temperature (19−21). Higher sensitivity requires that the time of transit is long, which is promoted by the low mobility. At the same time, a higher carrier concentration ensures less resistive transport and enhanced charge injection. Because the polymers are made of low-*Z* elements

* E-mail: hekatz@jhu.edu.
Received for review October 12, 2008 and accepted December 30, 2008
DOI: 10.1021/am8001132

Published on Web 02/02/2009

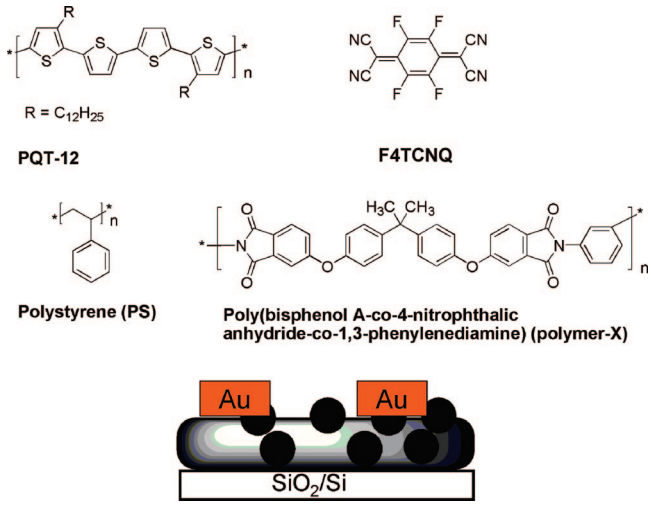

FIGURE 1. Molecular structures of blend composites and a schematic of the thin film transistor.

(such as C, N, H, and S), they have a natural advantage for spin devices, owing to the negligible spin−orbit interactions. The development of environmentally stable (resistant to O_2 and H_2O) polymers that meet these particular electrical property requirements is one of the long-term objectives of our studies. In this work, by blending a polythiophene, namely, poly(3,3‴-didodecylquaterthiophene) (PQT-12; Figure 1) with different kinds of insulating polymers and dopant concentrations, a very large range of mobility and conductivity can be obtained in a somewhat decoupled fashion.

We first studied a series of blends of PQT-12 and PS, observing the morphology and the charge carrier mobility. The compositional dependence of the charge carrier mobility in blended composites was investigated in FETs. We demonstrated substantially increased mobility upon mixing with insulating PS compared to pure PQT-12. We also demonstrated that low-mobility ($\sim 10^{-5}$ $cm^2/V \cdot s$) and high-conductivity (10^{-4} S/cm) devices can be acquired from a blend of PQT-12/F4TCNQ with the polar and irregular insulating polymer poly(bisphenol A-*co*-4-nitrophthalic anhydride-*co*-1,3-phenylenediamine). There are complications in using such complex mixtures involving environmental stability and compositional heterogeneity, and these will be discussed.

EXPERIMENTAL SECTION

Materials. PQT-12 was synthesized by $FeCl_3$-mediated oxidative coupling polymerization (22). Polystyrene (a-PS, molecular weight = 13 000), poly(bisphenol A-*co*-4-nitrophthalic anhydride-*co*-1,3-phenylenediamine) (polymer-X), tetrafluorotetracyanoquinodimethane (F4TCNQ), hexamethyldisilazane (HMDS), and chlorobenzene (CB; anhydrous, 99%) were ordered from Aldrich. All materials were used without further purification.

Sample Preparation. ***PQT-12/PS.*** We prepared solution blends of PQT-12/PS as follows. PQT-12 and PS were each dissolved separately in CB. For a PQT-12 solution, an elevated temperature of 80 °C was used to achieve a complete solution. After cooling to room temperature, the PQT-12 solution was filtered through a 1 μm poly(tetrafluoroethylene) filter. Then the PQT-12 solution was mixed with different concentrations of PS solutions to finally form PQT-12/PS blend precursor solutions. For example, the blend composite that was obtained from 2 mg/mL of PQT-12 and 5 mg/mL of PS is defined as PQT-12/PS (2/5). The blend precursor solutions were sonicated for 5 min before use.

PQT-12/Insulator Polymer/F4TCNQ. We prepared solutions of PQT-12/insulator polymer/F4TCNQ as follows. F4TCNQ, insulator polymer (PS or polymer-X), and PQT-12 were first dissolved separately in CB. For the F4TCNQ solution, stirring and heating of the solution up to 80 °C was needed because of the limited solubility of F4TCNQ in CB. Immediately upon mixing of PQT-12, insulator polymer, and F4TCNQ, the color of the solution changed to black, while the pristine PQT-12 solution had been brown-red.

Devices. ***PQT-12/PS Devices.*** Top-contact organic field effect transistor devices were fabricated on HMDS-treated, heavily *n*-doped silicon wafers including a 300 nm thermally grown gate oxide layer. Whole substrates were cleaned by a piranha solution [H_2SO_4/H_2O_2 (1:3); **Danger!** *Highly oxidizing and corrosive*] and then treated with HMDS vapor for 2 h at 100 °C. Then PQT-12/PS blend precursor solutions, which had been sonicated for 5 min, were spin-cast (2000 rpm, 60 s) onto silicon wafers. For the source and drain electrode (channel length 250 μm; channel width 6 mm), ca. 50 nm of gold was deposited on top of the film using physical vapor deposition at 5×10^{-6} mbar at a rate of 0.5 Å/s. After gold film deposition, the device was baked in a vacuum oven at ca. 95 °C for 1 h and then slowly cooled to room temperature.

PQT-12/Insulator Polymer/F4TCNQ Devices. Top-contact devices were fabricated on heavily doped silicon wafers including 300 nm SiO_2. For the intentional fabrication of low-mobility devices, substrates were cleaned with acetone and isopropyl alcohol for 15 min and then dried on a hot plate for 2 h at 150 °C. Then a PQT-12/insulator polymer/F4TCNQ blend precursor solution was spin-cast (2000 rpm, 60 s) onto silicon substrates. Approximately 50 nm of gold was deposited on top of the film as the source and drain electrode. After gold film deposition, the film was kept in a desiccator for 24 h before measurement.

Characterization. ***Atomic Force Microscopy (AFM) Measurements.*** The AFM measurements were performed with a Pico Plus scanning probe microscope (Agilent Co.) operated at room temperature. A silicon tip with a resonance frequency of ~70 kHz and a scan rate of 1 Hz were used. All AFM measurements were operated in the tapping mode, which acquires topographical and phase images at the same time. The phase contrast essentially arises from the difference of energy dissipation during the tip−sample interaction. This enables it to differentiate between areas with different viscoelastic properties (23−25).

X-ray Photoelectron Spectroscopy (XPS) Measurements. XPS was measured by a Kratos Axis Ultra spectrometer. Al Kα (1486 eV), which was operated at 15 kV and 20 mA, was used to acquire the spectra under a vacuum of 1×10^{-6} Torr. A depth profile was obtained by etching the film with a Ar^+ gun (3.0 keV).

X-ray Diffraction (XRD) Measurements. XRD measurements (Philips X Pert Pro) were performed along the surface normal axis for all devices to understand the degree of crystallization of semiconductor films.

Differential Scanning Calorimetry (DSC) Measurements. DSC measurements were carried out by using a TA DSC Q20 modulated instrument at a heating and cooling rate of 10 °C/min under a nitrogen atmosphere.

Device Measurements. Direct current characteristics of the devices were obtained using a semiconductor parameter analyzer (Agilent 4155C). Output characteristics were obtained at a constant gate voltage $V_G = -100$ V and transfer characteristics at a constant drain voltage $V_{sd} = -100$ V. The current I_D modulated by V_G is approximately determined from the following equations:

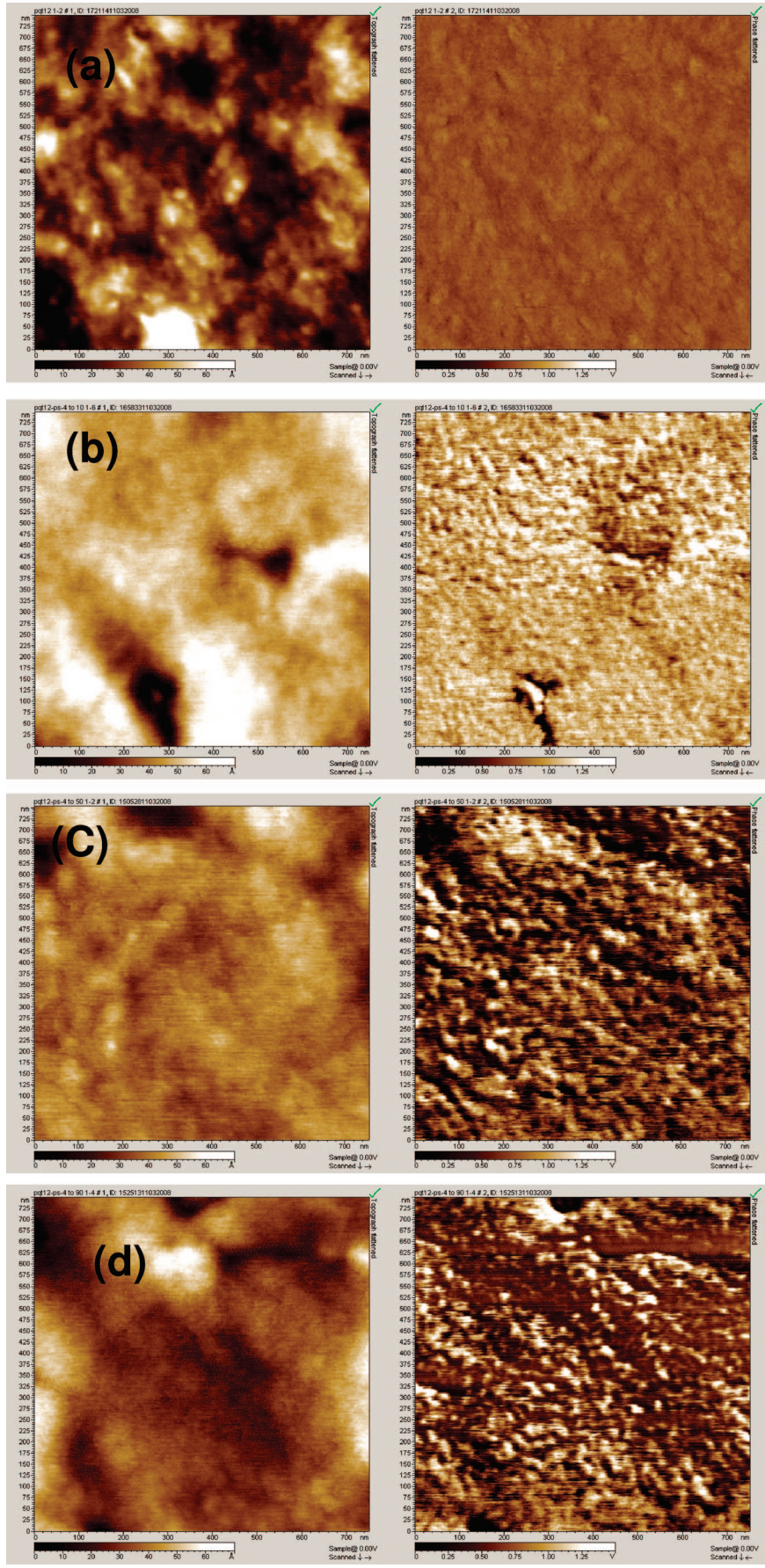

FIGURE 2. 750 nm × 750 nm AFM topographic (left column) and phase (right column) images of PQT-12 and a PQT-12/PS composite deposited on a HMDS-modified SiO_2 substrate. (a) PQT-12 film, (b) PQT-12/PS (2/5), (c) PQT-12/PS (2/25), and (d) PQT-12/PS (2/45) films were annealed at 95 °C for 1 h followed by slow cooling to room temperature.

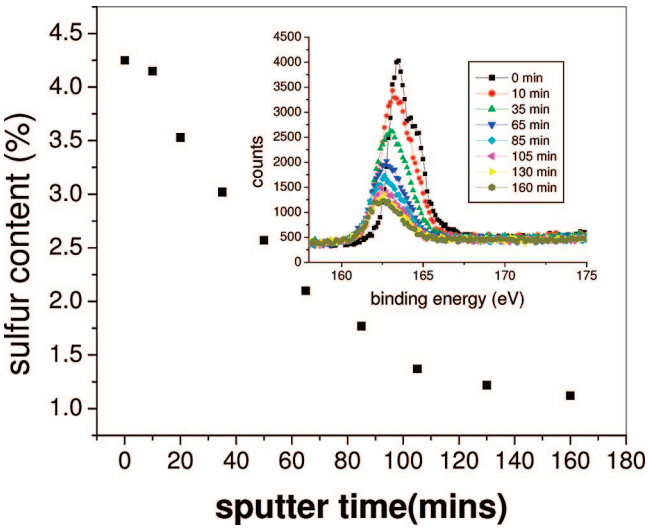

FIGURE 3. Sulfur content measured by XPS as a function of the Ar^+ sputter time. Inset: changes of S 2p in XPS spectra with the sputter time for a PQT-12/PS blend (2/5).

$$I_D = (W/L)C_i\mu(V_G - V_T)V_D \quad \text{(linear region)} \qquad (1)$$

$$I_D = (W/2L)C_i\mu(V_G - V_T)^2 \quad \text{(saturation region)} \qquad (2)$$

where μ is the field-effect mobility, L is the channel length (250 μm), W is the channel width (6 mm), C_i is the insulator capacitance per unit area, and V_T is the extrapolated threshold voltage, in some cases highly in the depletion regime. In such cases, the charge density per unit area equals V_TC_i. In the linear region, we used eq 1 to estimate the charge carrier mobility (μ) by plotting I_D versus V_G. In the saturation region, we used eq 2 to estimate the charge carrier mobility (μ) by plotting $(I_D)^{1/2}$ versus V_G. The electrical conductivity of the polymer blend was studied by two-probe $I-V$ measurement using gold as both electrodes. The bulk conductivity is determined from Ohm's law:

$$\sigma = LI/WVd \qquad (3)$$

where L and W are the channel length and width, respectively, and d is the polymer film thickness. Conductivity divided by mobility provides an alternative method of estimating the charge density.

RESULTS AND DISCUSSION

Transistors Based on PQT-12/PS Blends. Figure 2 presents AFM images of topography and phase acquired fabrication of large area active matrix displays on PQT-12 and a PQT-12/PS blend, each having been annealed at 95 °C. For the AFM topographic image of the PQT-12 homopolymer (Figure 2a), only nanosized crystallites containing a small number of stacked molecules can be observed. The surface roughness of the film could be measured directly from the topographic image to be about 1.1 nm. The phase image of the PQT-12 homopolymer does not show any high-contrast features, indicating only disordered packing of PQT-12 on the SiO_2 substrate (26). Upon the addition of PS into PQT-12 (Figure 2b–e), morphologies become smoother and featureless and the roughness of the blends is <1 nm. The phase images of the PQT-12/PS composite are highly informative because they clearly show distinct phases of PQT-12 and PS. The light spherical domains in the phase images of PQT-12/PS decrease in size with an increase in the fraction of PS, indicating that the light regions represent the PQT-12 phase. For the PQT-12/PS (2/5) blend film, light spherical domains that formed a continuous fibril network are observed, suggesting that with this special blend ratio the top-layer of the PQT-12/PS composite is enriched in a continuous mat of PQT-12. This would be expected to be advantageous for maximizing the hole mobility. In the PQT-12/PS (2/25) and PQT-12/PS (2/45) composites, isolated spherical, clusterlike domains (~30 nm in diameter) that are associated with PQT-12 can be observed. Number of such domains decreases with an increase in the fraction of PS and the length of any single domain is about 200 nm.

We further investigated the cross section of a PQT-12/PS blend film. The composition of PQT-12/PS (2/5) as a function of the depth was analyzed by XPS combined with argon sputtering (Figure 3). The sulfur content, which indicates the relative amount of PQT-12, showed a depth-dependent character in the PQT-12/PS blend film. Before argon sputtering, a sulfur content of 4.46%, associated with the amount of PQT-12 at the top layer of the PQT-12/PS composite, was observed. This value is close to that of the sulfur content of 6.46% obtained from a pure PQT-12 film, consistent with the formation of a PQT-12-rich top layer. During argon sputtering, it can be seen that the sulfur content decreases with the sputter time. After sputtering for 160 min (sufficient to remove approximately 80% of the film), the surface sulfur content decreased from 4.46% to 1.12%, which indicates that vertical phase separation has occurred in the PQT-12/PS film. This leads to PQT-12 enrichment on the top layer of the PQT-12/PS composite and PS enrichment on the bottom layer of the PQT-12/PS composite. The reason for vertical phase separation of the PQT-12/PS composite may be related to the preferential adsorption of relatively hydrophobic PS to the HMDS-modified SiO_2 substrate. Similar results are observed in many nonconjugated polymer blends (27–29). From the Figure 3 inset, it also can be seen that the binding energy (BE) of S 2p shifted significantly to a lower BE with increased sputter time. Because the BE of C 1s shifted correspondingly to lower BE with increased sputter time (not shown), it can be concluded that this change is related to Ar^+ trapping at the surface or in the bulk of the PQT-12/PS composite with increased sputter time.

The electronic performances in the FET device configuration of a PQT-12 film and a PQT-12/PS composite are shown in Figure 4a–c. Both fabrication and measurement were carried out under ambient conditions. The field-effect mobility calculated from the saturated region of the PQT-12 film is 4×10^{-3} $cm^2/V \cdot s$ with a corresponding on/off ratio of 3×10^4. However, for the PQT-12/PS (2/5) blend, the field electric mobility is 8×10^{-2} $cm^2/V \cdot s$ with an on/off ratio of 10^5. It is interesting to observe that PQT-12/PS (2/5) showed substantially increased mobility compared to pure PQT-12. The detailed dependence of the field-effect mobility on the PS content is shown in Figure 4d. The field-

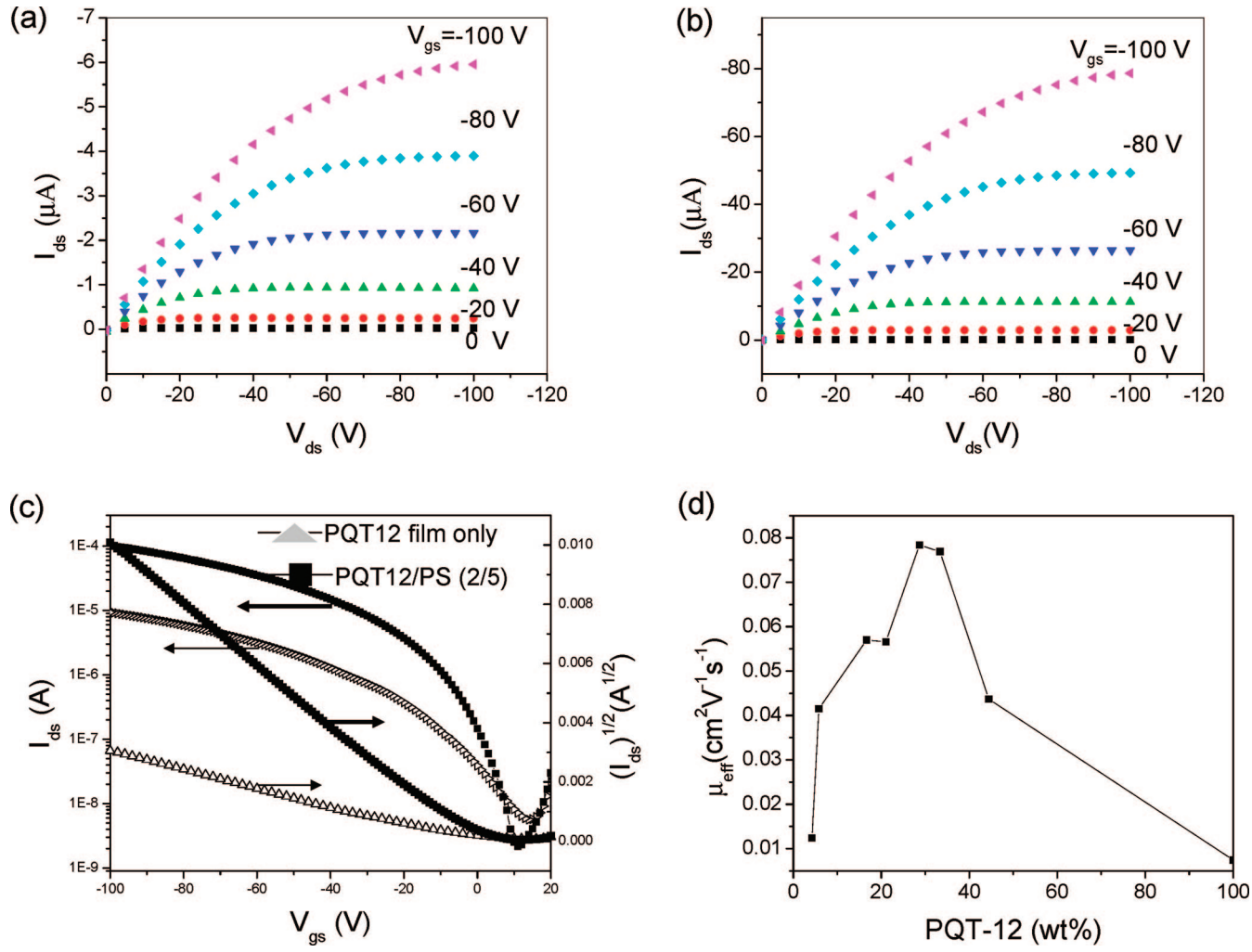

FIGURE 4. Output and transfer characteristics of a PQT-12/PS blend. (a) Output characteristic of a PQT-12 film. (b) Output characteristic of a PQT-12/PS (2/5) blend device. (C) Transfer characteristic of PQT-12 and a PQT-12/PS (2/5) blend. (d) Dependence of the field-effect mobility measured from a saturated region as a function of the PQT-12 content in blends with PS.

effect mobility of PQT-12/PS showed two different regimes as the PS content increased. First, the mobility of the blends rapidly increased to a maximum of 8×10^{-2} cm^2/V · s as the PS content increased from 0% to 67%. Second, the mobility decreased as the PS continued to increase from 67% to 98%. It can be seen that PQT-12/PS blends have charge carrier mobility equal to or higher than the pure PQT-12 film, even when the semiconductor PQT-12 is present in nominal volume fractions of just 5−10%.

The enhanced mobility of a PQT-12/PS composite could be ascribed to the relatively hydrophobic PS at the bottom of the PQT-12/PS composite (30). However, because the SiO_2 substrate had been modified by HMDS before device fabrication, it was already fairly hydrophobic even without involvement of PS. In order to further understand this enhanced mobility of the PQT-12/PS composite film, PQT-12 homopolymer and a PQT-12/PS composite were analyzed by a combination of DSC and electronic characterization in the FET device configuration. DSC thermograms of PQT-12, PS, and PQT-12/PS (2/5) are first shown in Figure 5a. For the PQT-12/PS (2/5) composite, two peaks at 105 °C and 140 °C, which are related to PS and PQT-12, respectively, can be observed. For the pure PS, one T_g at ∼95 °C can be observed. For the pure PQT-12 film, two T_c's at ∼120 and ∼140 °C, corresponding respectively to crystal-to-liquid crystal and liquid crystal-to-isotropic phase transitions, are observed. The PQT-12 homopolymer, when spun from a solution at room temperature, exhibited a great tendency to form self-organized π stacks (22), but these were only nanosized. In our experiment, when the annealing temperature of PQT-12 is kept at 95 °C, below the crystal-to-liquid crystal phase temperature, a low hole mobility is observed. Increasing the annealing temperature up to the melting region (∼145 °C) followed by slow cooling down to room temperature disrupts the kinetic π stacking between polymer backbones and completely relaxes the chains to allow formation of a long-range-ordered π-stacking structure (26). Figure 5b presents the electronic performance in the FET device configuration of the PQT-12 film, annealing up to the melting region and then slow cooling to room temperature, The field-effect mobility calculated from the saturated region of the PQT-12 film is 3.38×10^{-2} cm^2/V · s with a corresponding on/off ratio of 3×10^4. In contrast, for the FET performance of the PQT-12/PS composite as a function of the annealing temperature (Figure 5c), a relatively low mobility (∼10^{-5} cm^2/V · s) was acquired from a sample

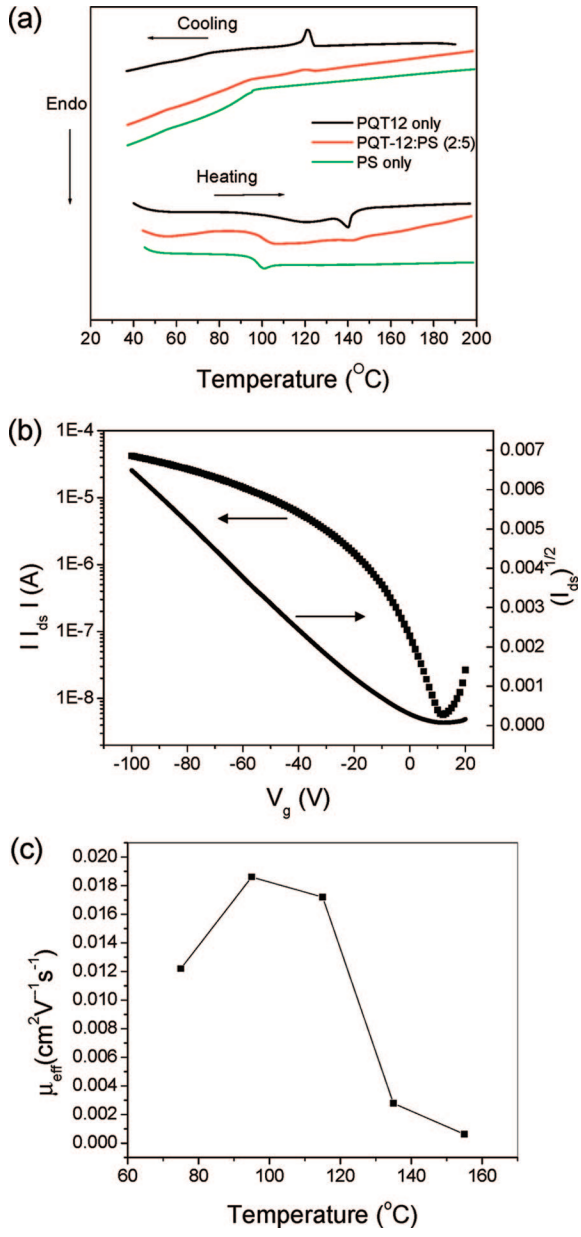

FIGURE 5. (a) DSC thermograms of PQT-12, PS, and the PQT-12/PS (2/5) blend. (b) Output characteristic of a PQT-12 device annealed at 135 °C. (c) FET performance of the PQT-12/PS (2/45) composite as a function of the temperature.

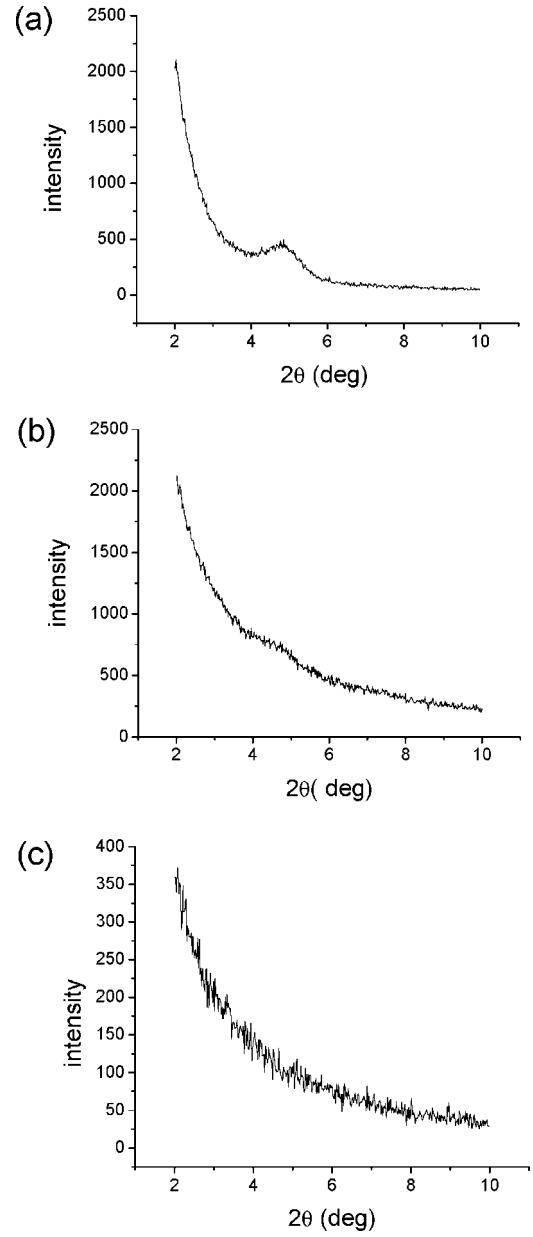

FIGURE 6. (a) XRD spectra of the PQT-12/PS (2/5) blend, showing a distinctive crystalline peak at $2\theta = 5.0°$. (b) XRD spectra of a PQT-12 film annealed at 95 °C, with no peak observed. (c) XRD spectra of a PS film annealed at 95 °C.

annealed at ~140 °C. However, for annealing at 95 °C, which coincided with the glass temperature of PS, a significant increase in the mobility by 1 or 2 orders of magnitude is observed. Because the annealing temperature (95 °C) for PQT-12/PS is far below T_c of PQT-12, annealing at this temperature is unlikely to improve the crystalline phase of pure PQT-12 for high field-effect mobility. However, because the glass transition temperature for PS is around 95 °C, molecular motions near the PQT-12/PS interface could result in a locally annealed, more crystalline PQT-12 domain.

In order to test further whether PS improves the structural order of PQT-12 films, XRD spectra of the PQT-12 homopolymer, PS only, and the PQT-12/PS composite on SiO_2 substrates, annealed at 95 °C, are shown in Figure 6. For the PQT-12/PS composite, there is a very distinctive crystalline peak at $2\theta = 5.0°$, which are not observed from the pure PS film or the PQT-12 film. The reflection peak at $2\theta = 5.0°$, which corresponds to an intermolecular distance of 18.0 Å, was due to the lamellar ordering between polymer backbones (31). The presence of the XRD peak in the PQT-12/PS composite at 95 °C affirmed the enhanced interchain crystallinity of PQT-12 within the PS matrix resulting from annealing at 95 °C.

Mobility and Conductivity Tuning. Results so far have demonstrated relatively high charge carrier mobility with low conductivity. It order to access a large range of conductivity and charge carrier mobility values for PQT-12 blend composites, F4TCNQ was used to p-dope PQT-12. Here, p-doping refers to the formation of charge-transfer complexes by electron transfer from the HOMO

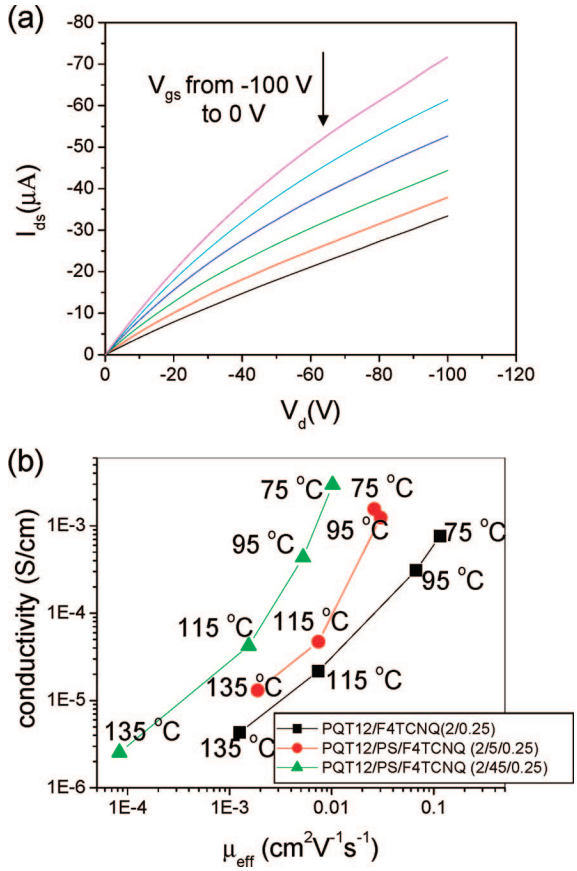

FIGURE 7. (a) Output characteristic of a PQT-12/F4TCNQ (4/0.5) blend device. (b) Field-effect mobility measured as a function of the conductivity in different kinds of polymer composites with different annealing temperatures.

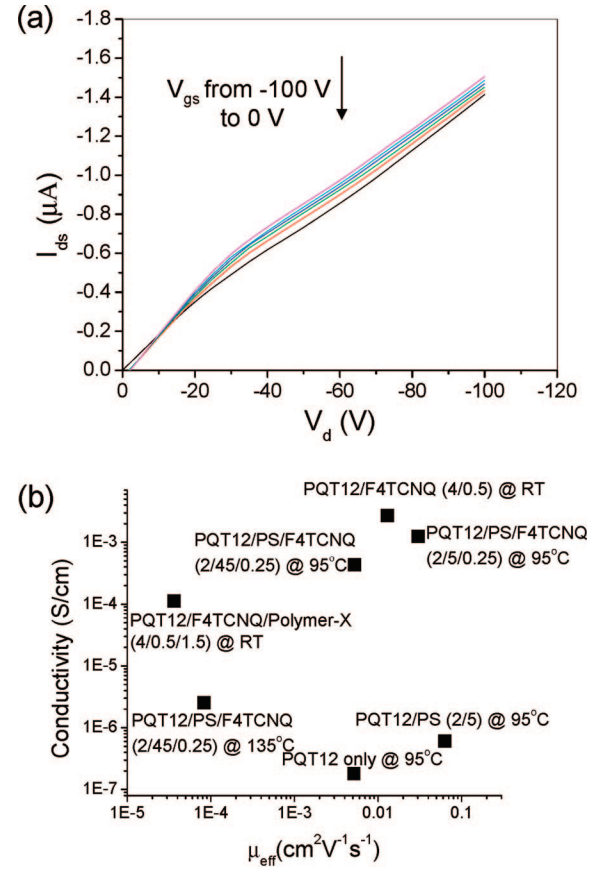

FIGURE 8. (a) Output characteristic of a PQT-12/F4TCNQ/polymer-X (4/0.5/1.5) blend device. (b) Dependence of the field-effect mobility measured as a function of the conductivity in a PQT-12/insulating polymer composite.

level of the polymer to the LUMO of F4TCNQ. p-doping of a variety of conjugated polymers by F4TCNQ was studied by Yim et al. (32); they observed that conductivity values increase significantly with F4TCNQ doping and further with an increase in the percentage of doping. Doping results in a several orders of magnitude increase in the bulk conductivity. The same trend is also observed for PQT-12 doped by F4TCNQ. For example, the electronic performance in the FET device configuration of PQT-12/F4TCNQ (4/0.5) is shown in Figure 7a. The FET mobility calculated from the linear region of PQT-12/F4TCNQ is 1.29×10^{-2} $cm^2/V \cdot s$, with a conductivity of 2.73×10^{-3} S/cm.

Ironically, it proved much more challenging to fabricate a high conductivity/low mobility device, and we tried a variety of approaches. For example, as noted above, PQT-12 combined with mobile PS gave a relatively low mobility. The field-effect mobilities measured as a function of the conductivity in different kinds of PQT-12/F4TCNQ/PS polymer composites with different annealing temperatures were studied and are summarized in Figure 7b. A very large range of mobilities and conductivities were obtained in a somewhat coupled fashion: the mobility of the polymer composite gradually decreased from 10^{-2} to 10^{-5} $cm^2/V \cdot s$, and at the same time, the conductivity of films also gradually decreased from 10^{-3} to 10^{-6} S/cm. However, high conductivity/low mobility devices still could not be obtained from this material system.

Finally, we turned to a more polar and more structurally inhomogeneous insulating polymer, polymer-X, as the blending agent to dilute the mobility of PQT-12 polymers. We reasoned that this irregular and incompatible polymer would increase the disorder of the PQT-12 domains, unlike the hydrocarbon polymers had done. We further added dopant (F4TCNQ) in order to increase the conductivity. The electronic performance in the FET device configuration of a PQT-12/F4TCNQ/polymer-X (4/0.5/1.5) film is shown in Figure 7b. The effective mobility from this device is only 3.62×10^{-5} $cm^2/V \cdot s$; however, the measured conductivity of the device is 1.12×10^{-4} S/cm. It is clear that this strategy succeeds in preventing the formation of the separate, continuous high-mobility phase because the mobility is drastically lower even as the dopant does indeed increase the conductivity and therefore the charge density. The field-effect mobility measured as a function of the conductivity in different kinds of PQT-12-insulating polymer composites is summarized in Figure 8b. All field-effect mobilities were calculated from the linear regions. The figure clearly shows the large range of conductivity (from 10^{-7} to 10^{-3} S/cm) and charge carrier mobility (from 10^{-5} to 10^{-2} $cm^2/V \cdot s$) values that can be acquired from various PQT-12 blend composites. The high conductivity/low mobility combination of properties meets the assumed requirements for

ultrasensitive magnetic sensor applications. However, we find that the measured properties change with time, arising most likely from autodoping of O_2 and H_2O from the environment, and considerable drift is observed in the current−voltage curves when acquired over hours to days in air. Devices are stabilized over days to weeks if stored under dry nitrogen. Means of hardening/cross-linking the polymers and/or packaging them with hermetic coatings will be developed to allow their ultimate utilization.

Summary. Mobility and conductivity can be tuned over large ranges in PQT-12 blends. The mobility of PQT-12 devices can be improved by PQT-12 and PS blending. Phase separation occurs in the PQT-12/PS film, which leads to high PQT-12 content on the top layer of the PQT-12/PS composite and a mostly PS composite on the bottom layer. The PQT-12 phase in PQT-12/PS composites is changed from disordered packing of PQT-12 to isolated spherical, clusterlike features with increasing PS content. In addition, the PQT-12 composite crystallizes at an annealing temperature of 95 °C, which was below the crystal-to-liquid crystal phase temperature of PQT-12 itself. The high mobility of PQT-12/PS composites may be useful for further plastic and printed electronics applications. For the low mobility and high conductivity device, blending polar, irregular insulating polymers into PQT-12 to dilute the mobility and adding dopant to increase the charge density gave a device with a mobility of $\sim 10^{-5}$ $cm^2/V \cdot s$ and a conductivity of 10^{-4} S/cm. This kind of device is of interest for spin-transport and magnetoresistance studies.

Acknowledgment. We acknowledge Drs. Zhi Gang Yu and Srini Krishnamurthy of SRI for their guidance on electrical requirements for polymers to be considered in spintronics applications and for collaboration on thin film conductivity testing. The authors thank Professor Peter Searson for use of an atomic force microscope. We also acknowledge use of the surface analysis laboratory at Johns Hopkins University (JHU) funded as part of the Materials Research Science and Engineering Center (MRSEC) through the National Science Foundation (NSF). This work was funded by SRI through a subcontract of an Office of Naval Research grant and also by the Petroleum Research Foundation, NSF (Grant ECS 0528472), and the Research Experiences for Undergraduates (REU) program of the MRSEC. We thank Professors Edmund Nowak of the University of Delaware for helpful discussions.

REFERENCES AND NOTES

(1) Dimitrakopoulos, C. D.; Mascaro, D. J. *Adv. Mater.* **2002**, *14*, 99.
(2) Sirringhaus, H.; Tessler, N.; Friend, R. H. *Science* **1998**, *280*, 1741.
(3) Sirringhaus, H.; Kawas, T.; Friend, R. H.; Shimoda, T.; Inbasekaran, M.; Wu, W.; Woo, E. P. *Science* **2000**, *290*, 2123.
(4) Shin, C.-K.; Lee, H. *Synth. Met.* **2004**, *140*, 177.
(5) Yu, G.; Gao, J.; Hummelen, J. C.; Wudl, F.; Heeger, A. J. *Science* **1995**, *270*, 1789.
(6) Yang, X.; Loos, J.; Veenstra, S. C.; Verhees, W. J. H.; Wienk, M. M.; Kroon, J. M.; Michels, M. A. J.; Janssen, R. A. J. *Nano Lett.* **2005**, *5*, 579.
(7) Friend, R. H.; Gymer, R. W.; Holmes, A. B.; Burroughes, J. H.; Marks, R. N.; Taliani, C.; Bradley, D. D. C.; Dos Santos, D. A.; Bredas, J. L.; Logdlund, M.; Salaneck, W. R. *Nature* **1999**, *397*, 121.
(8) Sirringhaus, H.; Brown, P. J.; Friend, R. H.; Nielen, M. M.; Bechgaard, K.; Langeveld-Voss, B. M. W.; Spiering, A. J. H.; Janssen, R. A. J.; Meijer, E. W.; Herwig, P.; de Leeuw, D. W. *Nature* **1999**, *401*, 685.
(9) Bao, Z.; Dodabalapur, A.; Lovinger, A. *Appl. Phys. Lett.* **1996**, *69*, 4108.
(10) McCullough, R. D.; Tritram-Nagles, S.; Williams, S. P.; Lowe, R. D.; Jayaraman, M. *J. Am. Chem. Soc.* **1993**, *115*, 4910.
(11) Yamamoto, T.; Komarudin, D.; Arai, M.; Lee, B. J.; Suganuma, H.; Asakawa, N.; Inoue, Y.; Kubota, K.; Sasaki, S.; Fukuda, T.; Matsuda, H. *J. Am. Chem. Soc.* **1998**, *120*, 2047.
(12) Arias, A. C.; Endicott, F.; Street, R. A. *Adv. Mater.* **2006**, *18*, 2900.
(13) Lu, G. H.; Tang, H. W.; Qu, Y. P.; Li, L. G.; Yang, X. N. *Macromolecules* **2007**, *40*, 6579.
(14) Goffri, S.; Muller, C.; Stingelin-Stutzmann, N.; Breiby, W. D.; Radano, C. P.; Anderasen, J. W.; Thompson, R.; Janssen, R. A. J.; Nielsen, M. M.; Smith, P.; Sirringhaus, H. *Nat. Mater.* **2006**, *5*, 950.
(15) Sauve, G.; McCullough, R. D. *Adv. Mater.* **2007**, *19*, 1822.
(16) Madec, M.-B.; Crouch, D.; Liorente, G. R.; Whittle, T. J.; Geoghegan, M.; Yeates, S. G. *J. Mater. Chem.* **2008**, *18*, 3230.
(17) Basescu, N.; Liu, Z.-X.; Moses, D.; Heeger, A. J.; Naarmann, H.; Theophilou, N. *Nature* **1987**, *327*, 403.
(18) Aziz, E. F.; Vollmer, A.; Eisebitt, S.; Eberhardt, W.; Pingel, P.; Neher, D.; Koch, N. *Adv. Mater.* **2007**, *19*, 3257.
(19) Yu, Z. G.; Berding, M. A.; Krishnamurthy, S. *J. Appl. Phys.* **2005**, *97*, 024510.
(20) Yu, Z. G.; Berding, M. A.; Krishnamurthy, S. *Phys. Rev. B (Rapid Commun.)* **2005**, *71*, 060408.
(21) Yu, Z. G.; Berding, M. A.; Krishnamurthy, S. *IEE Proc.-G: Circuits, Devices Syst.* **2005**, *152*, 334.
(22) Ong, B.; Wu, Y. L.; Liu, P.; Garden, S. J. *J. Am. Chem. Soc.* **2004**, *126*, 3378.
(23) Cleveland, J. P.; Anczykowski, B.; Schmid, A. E.; Elings, V. B. *Appl. Phys. Lett.* **1999**, *72*, 2613.
(24) Scottt, W. W.; Bhushan, B. *Ultramicroscopy* **2003**, *97*, 151.
(25) Marcus, M. S.; Eriksson, M. A.; Darryl, Y. S.; Carpick, R. W. *Ultramicroscopy* **2003**, *97*, 145.
(26) Zhan, N.; Bottom, G. A.; Zhu, S. P.; Duft, A.; Ong, B.; Wu, Y.-L.; Liu, P. *Macromolecules* **2004**, *37*, 8307.
(27) Boltau, M.; Walheim, S.; Mlynek, J.; Krausch, G.; Steiner, U. *Nature* **1998**, *391*, 877.
(28) Jones, R. A. L.; Norton, L. J.; Kramer, E. J.; Bates, F. S.; Wiltzius, P. *Phys. Rev. Lett.* **1991**, *66*, 1326.
(29) Walheim, S.; Boltau, M.; Mlynek, J.; Krausch, G.; Steiner, U. *Macromolecules* **1997**, *30*, 4995.
(30) Qiu, L. Z.; Lim, J. A.; Wang, X. H.; Lee, W. H.; Hwang, M.; Cho, K. *Adv. Mater.* **2008**, *20*, 1141.
(31) Ong, B. S.; Wu, Y.-L.; Liu, P.; Gardner, S. *Adv. Mater.* **2005**, *17*, 1141.
(32) Yim, K.-H.; Whiting, G. L.; Murphy, C. E.; Halls, J. M.; Burroughes, J. H.; Friend, R. H.; Kim, J.-S. *Adv. Mater.* **2008**, *20*, 3319.

AM8001132